# Kinetically driven ordering in phase separating alloys

Zhang, Xi; Sluiter, Marcel H.F.

**DOI**
10.1103/PhysRevMaterials.3.095601

**Publication date**
2019

**Document Version**
Final published version

**Published in**
Physical Review Materials

# Kinetically driven ordering in phase separating alloys

Xi Zhang and Marcel H. F. Sluiter*
*Department of Materials Science and Engineering, Delft University of Technology, Mekelweg 2, 2628 CD Delft, The Netherlands*

(Received 15 April 2017; revised manuscript received 16 July 2019; published 13 September 2019)

It is shown that in substitutional alloys, peculiar ordered patterns can result from neighborhood-dependent diffusion activation barriers even when there are no metastable ordered phases. Lattice gases with pure phase separation character are shown to exhibit transient ordered structures that can be retained almost indefinitely, although these structures are not at thermodynamic equilibrium. It is shown that such structures can come about relatively easily by quenching from the high-temperature configurationally random solid solution.

DOI: 10.1103/PhysRevMaterials.3.095601

## I. INTRODUCTION

The thermodynamic properties of the Ising model have been studied intensely for almost a century. The role of dimensionality, the occurrence of order-disorder transitions, and many other features of this model and its generalizations are now well understood [1,2]. Among the most interesting applications of the Ising model and its generalizations is the study of substitutional alloys [3–5]. With the advent of *ab initio* methods to compute the effective interatomic interactions, the practical utility of the model has greatly expanded [6–12]. When the generalized Ising model is applied to alloys, the kinetics of these alloys is at least as interesting as the study of thermodynamic equilibrium. After all, real alloys are usually at a kinetically determined intermediary stage evolving toward thermodynamic equilibrium, rather than at equilibrium [13,14]. Kinetics in substitutional alloys generally is driven by vacancy-mediated diffusion. While vacancies, because of their typically low equilibrium concentration, rarely play a role in equilibrium thermodynamics, they are crucial for kinetics. Experimentally too, the intricate details of vacancy behavior in substitutional alloys has attracted attention again lately [15–19]. A number of studies exist on Ising model kinetics, some of which neglect vacancies [20] and therefore unrealistic kinetics, others which include vacancies but which employ simplifying assumptions concerning diffusion activation energies [21–23], and recently some studies where multiple issues surrounding vacancies and diffusion barriers are considered [24–28]. These latter studies generally appear able to provide realistic timescales and evolution histories. Here, we take a special interest in the evolution history, particularly the occurrence of transient phases [29–32].

We define transient phases as nonequilibrium phases that can occur during the evolution toward equilibrium for an extended, but finite, period of time. It is well understood that transient-ordered phases can form from a disordered, or randomlike, solid solution with unmixing tendencies if there are metastable ordered phases that are much more stable than the disordered solid solution, such as occur in various semiconductor alloys [33]. These observations have been explained in terms of strain energy minimization by atomic size mismatch [33–35]. Even in the absence of strain effects, metastable ordered phases can be transient, as has been found in Monte Carlo simulations of phase separating alloys [32,36–38] or in concentration wave simulations [39]. In all these cases, transient ordered phases appear under the constraint of limited atomic mobility; free energy can be reduced more quickly by metastable ordering than by macroscale phase separation. This explanation for the occurrence of transient phases has proven so alluring that, quite generally, transient phases in bulk alloys are ascribed to thermodynamic metastability, often in conjunction with limited atomic mobility [40–46]. The importance of purely kinetic effects in phase selection has been seen in colloidal system simulations [47] where metastable NaCl-type ordering occurs prior to, or instead of, stable CsCl type ordering. A less clear scenario occurs when preferred nucleation is in play, particularly when heterogeneous nucleation for a metastable phase happens more readily than nucleation of the stable phase [48]. However, here too, thermodynamic competition remains an important factor. Purely kinetic factors have not been reported for metallic alloys. With the increasing awareness that vacancy formation and substitutional diffusion in concentrated alloys is strongly dependent on the local environment [24,25,49–54], it is of interest to examine the impact of this local environment dependence of the kinetics.

In this paper, we report transient order in a configurationally random alloy upon quenching into the two-phase region pertaining to phase separation. Here, we show that without any thermodynamic causative factor, there also may be a purely kinetic origin of transient phases. Following a detailed description of our model (Sec. II), we analyze first a 2D case, and subsequently show that in 3D analogous phenomena occur as in 2D.

## II. THEORY AND MODEL DESCRIPTION

### A. Vacancy-mediated substitutional diffusion

The phase evolution described in the present paper results from vacancies trading places with neighboring atoms on a

*M.H.F.Sluiter@tudelft.nl

 

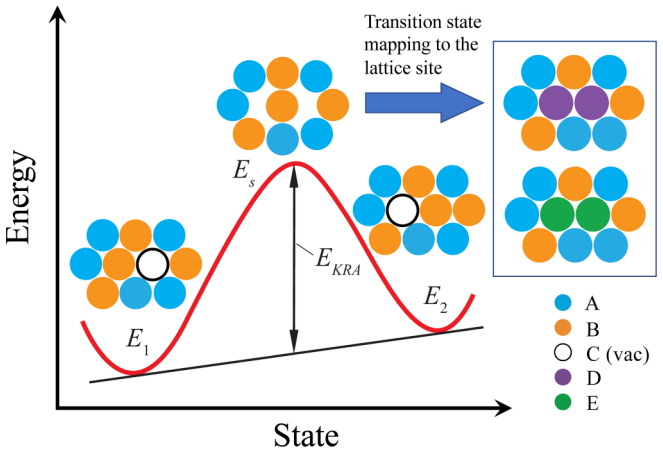


FIG. 1. Schematic description of the vacancy-mediated substitutional diffusion. The energy landscape is shown by the thick red curve where two valleys represent the energies of the two end points ($E_1$ and $E_2$) and the peak in between is the energy at the saddle point ($E_s$). The corresponding atomic configurations for a binary A-B alloy are also displayed. The kinetically resolved activation (KRA) barrier is illustrated by the black double-headed arrow. The configurations shown in the box illustrate the mapping of the jumping atom at the transition state on to the lattice site.

substitutional lattice, as is schematically shown in Fig. 1. Atomic movements, e.g., from state $E_1$ to $E_2$, must overcome a certain activation energy barrier. The kinetics of vacancy-atom swapping is generally modeled by the transition state theory, where the rate of the transition between state $i$ and $j$ is expressed by an Arrhenius relation,

$$r_{i\to j} = \omega \exp(-\beta Q(i \to j)), \tag{1}$$

where $\omega$ is the jump attempt frequency. For simplicity, we assume in the present paper that $\omega$ is configuration and temperature independent and takes a value of 1 THz. $\beta = 1/(k_B T)$, and $Q$ is the activation energy barrier which simply refers to the energy difference between the saddle point and the starting point (i.e., in Fig. 1 from left to right, $Q = E_s - E_1$). A problem then arises that the activation energy barrier is not a state function because it depends on the jump direction, i.e., $Q(1 \to 2) \neq Q(2 \to 1)$, as is illustrated in Fig. 1. This problem can be solved by using the so-called kinetically resolved activation (KRA) barrier [24,50] defined as

$$E_{\mathrm{KRA}} = E_s - \tfrac{1}{2}(E_i + E_j), \tag{2}$$

as shown in Fig. 1. Once the $E_{\mathrm{KRA}}$ and the configurational energies of the two end points ($E_i$ and $E_j$) are known, the transition rates are obtained by combining Eqs. (1) and (2):

$$r_{i\to j} = \omega \exp\big[-\beta\big(E_{\mathrm{KRA}} + \tfrac{1}{2}E_j^{\mathrm{conf}} - \tfrac{1}{2}E_i^{\mathrm{conf}}\big)\big]. \tag{3}$$

Here the superscript conf indicates the configurational energy. It is apparent that both the energetic ingredients for computing the transition rates—the KRA barriers $E_{\mathrm{KRA}}$ and the configurational energies $E_{i(j)}^{\mathrm{conf}}$—depend on chemical order in alloys. While the configurational energies represent the average energetics of alloys, the KRA barriers depend only on the local chemical order. Therefore, it is efficient to model and calculate them via two different types of cluster expansions (CEs).

### B. Conventional cluster expansions for the configurational energy

Intentionally, the simplest thermodynamic model is used with two atomic species A and B on a rigid lattice (a binary A-B alloy) with effective interatomic interactions limited to the nearest neighbors. The interactions favor phase separation into the pure constituents, but configurational entropy leads to intermixing as temperature is raised. Vacancies are treated as an additional species C and are assumed to have the same effective interactions with both atomic species, so their concentration is not dependent on (local) composition or order. If we assign the most abundant species to A, it follows that only effective cluster interactions (ECIs) associated with species B and C are necessary to fully describe the configurational energy because of the sum rules [53,54]. Then we elaborate the A-B-C CE to describe the configurational energy $E^{\mathrm{conf}}$ as

$$E^{\mathrm{conf}} = \sum_{\alpha=1}^{2} n_\alpha^{\mathrm{ABC}} J_\alpha^{\mathrm{ABC}}, \tag{4}$$

where $\alpha$ indicates a particular cluster, $\alpha = 1(2)$ refers to the B point cluster (B-B nearest-neighbor pair), $n_\alpha$ is a counter for the number of $\alpha$-type clusters per lattice site, and $J_\alpha$ is the corresponding ECI. To keep the model as simple as possible, the vacancy interactions between C and A, and C and B are all the same and equal to zero. The vacancy prefers neither A nor B neighbors. The vacancy formation energy is not of concern because we impose that there is but a single, conserved, vacancy in our system.

We first consider a square lattice (2D) with nearest-neighbor interactions only. To see if transient order occurs without there being a metastable ordered structure lurking just above the convex hull of ground states, We arbitrarily select $J_1^{\mathrm{ABC}} = +0.8$ eV/point and $J_2^{\mathrm{ABC}} = -0.4$ eV/pair, so that $E^{\mathrm{conf}}$ is a parabola as function of the composition with a maximum of $+0.2$ eV/atom in the random equiatomic A-B alloy, and $E^{\mathrm{conf}} = 0$ eV for pure A and pure B. These interactions give rise to a miscibility gap with a critical temperature of about 2633 K at equiatomic composition [55]. Then, for an fcc lattice, we selected interactions in a similar fashion as for the square lattice. The corresponding ECIs are $J_1^{\mathrm{ABC}} = +1.2$ eV/point and $J_2^{\mathrm{ABC}} = -0.2$ eV/pair.

### C. Local cluster expansions for kinetically resolved activation barriers

For expanding the KRA barriers $E_{\mathrm{KRA}}$ in Eq. (3) by local cluster expansions (LCEs), special treatment is necessary because in the transition state the jumping atom is no longer uniquely associated with a single lattice site (see the configuration associated with $E_s$ in Fig. 1). To retain the fixed lattice gas approximation, with there being one and only one atomic species per site, we employ the formalism of Ref. [54]. Two new atomic species D and E are introduced that map the jumping atom at the transition state onto the lattice sites, as shown in the boxed area of Fig. 1. More specifically, at the transition state, the pair of the jumping atom A (B) and

its neighbor vacancy C [A-C (B-C) pair] is replaced with a new "pseudoatomic pair" D-D (E-E). A great simplification can be made if we assume that within our material vacancies are so rare they never exist within each others vicinity. Then, the C, D, and E species can never occur simultaneously and their interactions are not needed. As a result, only two new ternary LCEs A-B-D and A-B-E are necessary for describing the A and B atom in the transition state, respectively. The corresponding KRA barriers are expressed as

$$E_{\mathrm{KRA}}^{\beta\cup\gamma} = J_{\beta}^{\mathrm{ABX}} + \sum_{\gamma} n_{\beta\cup\gamma}^{\mathrm{ABX}} J_{\beta\cup\gamma}^{\mathrm{ABX}}, \; X = \mathrm{D}, \mathrm{E}, \tag{5}$$

where $J_{\beta}^{\mathrm{ABX}}$ is the KRA barrier for the jumping atom purely surrounded by the most abundant species (A atom in the present cases), $\beta$ represents the pseudoatomic pair, $\gamma$ represents a cluster configuration corresponding to the empty cluster, or a point cluster, etc. but not part of the pseudoatomic pair, $n_{\beta\cup\gamma}^{\mathrm{ABX}}$ is a counter for the number of cluster decorations of type $\beta\cup\gamma$, and $J_{\beta\cup\gamma}^{\mathrm{ABX}}$ is the corresponding ECI. To geometrically distinguish different correlation functions, the whole "pseudoatomic pair" $\beta$ is included when selecting the correlation functions, as discussed in Ref. [54]. We apply the above-described formalism for KRA barriers again first to a 2D square lattice and then to the fcc lattice.

For the 2D square lattice, we again try to make the case as simple as possible: For all configurations around a D-D pair, $E_{\mathrm{KRA}} = 0.7\,\mathrm{eV}$. It follows that $E_{\mathrm{KRA}}$ for a majority A atom trading places with a vacancy is always 0.7 eV. For the B-atom diffusion, on the other hand, we opt here for configuration dependence via an A-B-E LCE. We set $J_{\beta}^{\mathrm{ABE}} = 0.6\,\mathrm{eV}$ for the KRA barrier of a B atom surrounded purely by A atoms and use four cluster decorations of $\beta\cup\gamma$ labeled 1 through 4 shown in Fig. 2.

The environment-dependent KRA barriers for configurations of $\gamma = 1$ to 4 shown in Fig. 2 can be computed using the corresponding ECIs as

$$\begin{aligned}
E_{\mathrm{KRA}}^{\beta\cup1} &= J_{\beta} + J_1 = 0.6 - 0.1 = 0.5,\\
E_{\mathrm{KRA}}^{\beta\cup2} &= J_{\beta} + J_1 + J_2 = 0.6 - 0.1 + 0.7 = 1.2,\\
E_{\mathrm{KRA}}^{\beta\cup3} &= J_{\beta} + J_3 = 0.6 - 0.05 = 0.55,\\
E_{\mathrm{KRA}}^{\beta\cup4} &= J_{\beta} + J_1 + 2J_2 + J_4\\
&= 0.6 - 0.1 + 2\times 0.7 - 0.7 = 1.2,
\end{aligned} \tag{6}$$

where the number in the subscript of $J$ indicates the value of $\gamma$.

The included clusters and their associated ECIs have been chosen carefully. To simplify the model, we show the formation of a simplest ordered structure—linear arrays—of the minority atom (B atom). The origin of the kinetically driven ordering is essentially the selective movement of the diffusing atoms driven by the nonuniform KRA barriers. The clusters of the types that promote the formation of a linear array of B atoms, e.g., $\gamma = 1$ and 3, which enhance the attachment of two separate B atoms or a branch B atom to an existing B-B pair, are selected with lower barriers ($E_{\mathrm{KRA}}^{\beta\cup1} = 0.5$ and $E_{\mathrm{KRA}}^{\beta\cup3} = 0.55$) than the majority of the KRA barriers [i.e., environment independent barriers for diffusing atoms A (0.6 eV) and B (0.7 eV)]. However, these favorable KRA barriers should not be set too low because then many back-and-forth oscillations occur without the actual configuration evolving, e.g., between states $p_2$ and $p_3$ in Fig. 3. Fortunately, to a large degree such "unproductive oscillations" can be integrated out by using the absorbing Markov chain algorithm [56]. Figure 3 also illustrates the principle of kinetic ordering: While the lowest energy occurs for the vacancy jumping toward position $p_1$, the transient state represented by position $p_4$ is more likely

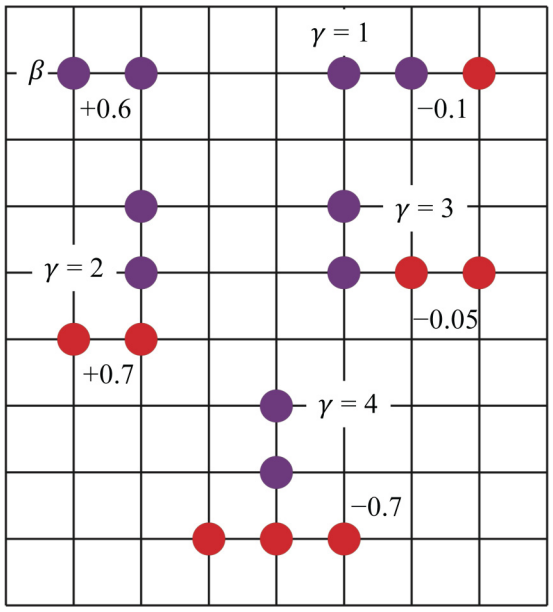


FIG. 2. Clusters and effective cluster interactions used for expanding the configuration dependence of the KRA barriers on the 2D square lattice. Cluster types $\beta$ and $\gamma$ and their associated ECIs (in eV/cluster) are indicated next to each configuration. Red circles indicate B species, purple circles E species, and A species are present at all grid points, but are not drawn for clarity.

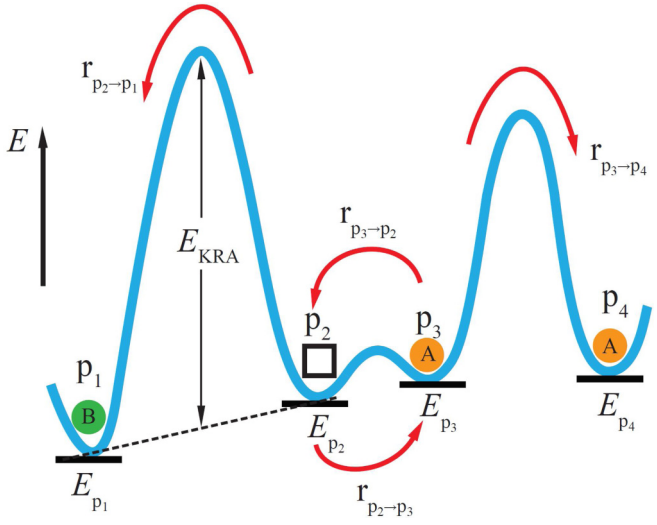


FIG. 3. Schematic diagram of an energy landscape with low barriers between states 2 and 3. Black square represents a vacancy, species C, while orange and green solid circles refer to atomic species A and B.

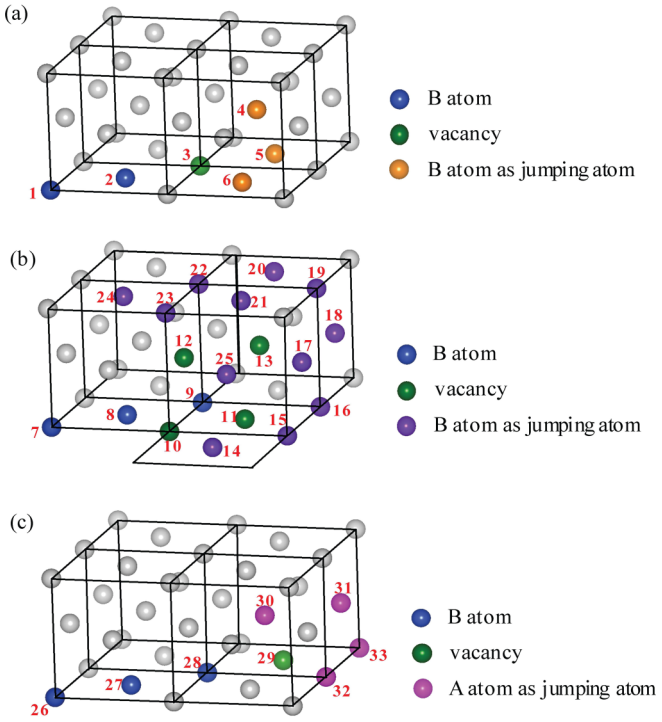


FIG. 4. Illustration of the clusters ($\gamma$) and the corresponding decorations used in the local cluster expansions A-B-D and A-B-E for (c) A atom and (a), (b) B atom as the jumping atom. The number displayed next to each colored atom is used for describing the corresponding clusters in Table I. Fcc cubes (black solid lines) have been added for clarity.

to be reached within short time spans. The other clusters, i.e., $\gamma = 2$ and 4, are selected yielding a much higher KRA barrier of 1.2 eV to limit the growth of side branches on such linear B arrays.

For the fcc lattice, the selected clusters and their ECIs are shown in Fig. 4 and Table I, respectively. Unlike the 2D case, where we make the KRA barriers for B-atom diffusion environment-dependent only, here the KRA barriers for both A and B atom diffusion depend on the local chemical order. In Fig. 4, clusters $\beta \cup \gamma$ are shown formed by atoms that are numbered and that are not colored grey. The clusters are formed by four or five atomic species which can be read from the number sequence in the first column of Table I. The "pseudoatomic pair" $\beta$ = D-D or E-E for each cluster is instead shown by the actual atomic species in alloys, i.e., the jumping atom and the vacancy. The KRA barriers for an A atom ($J_\beta^{\mathrm{ABD}}$) and a B atom ($J_\beta^{\mathrm{ABE}}$) trading places with the vacancy when they are surrounded purely by A atoms are set to +0.8 eV and +1.0 eV, respectively. We try to exemplify the kinetically driven ordering on the fcc lattice via the formation of linear arrays of B atoms on the fcc {111} planes along ⟨110⟩ close-packed directions. Once there are two or more B atoms neighboring one another along a ⟨110⟩ direction, the KRA barriers for further growth at the ends of such a B-string become lower, so further growth is promoted. At the same time, KRA barriers for side branching from such a B string become higher. It follows that the $\gamma$ part of each selected cluster consists of two or three B atoms aligned along the ⟨110⟩ direction as shown by the blue atoms, e.g., 1–2 or 7–8–9. The cluster decorations shown in Fig. 4(a) have negative ECIs because they all enhance the third B atom connecting to the B-B pair in ⟨110⟩ while in Fig. 4(b) the ECIs are all positive to decrease the tendency toward branch growth. Clusters used in Fig. 4(c) with all negative ECIs accelerate the growth of the linear arrays by increasing the chance of forwarding the nearby vacancy to the front of the line once there is an A atom attached to the line.

TABLE I. Effective cluster interactions (ECIs) in A-B-D and A-B-E local cluster expansions for kinetically resolved activation (KRA) barriers. Numbers connected by – indicate a cluster $\beta \cup \gamma$. The positions of the atoms within each cluster can be found in the corresponding Figure column.

| Cluster for B atom diffusion | Figure | ECI (eV/cluster) |
|---|---|---|
| 1-2-3-4 | 4(a) | −0.3 |
| 1-2-3-5 | | −0.2 |
| 1-2-3-6 | | −0.25 |
| 7-8-9-10-14 | | |
| 7-8-9-10-25 | | |
| 7-8-9-11-15 | | |
| 7-8-9-11-16 | | |
| 7-8-9-11-17 | | |
| 7-8-9-11-25 | | |
| 7-8-9-12-21 | | |
| 7-8-9-12-22 | | |
| 7-8-9-12-23 | 4(b) | 0.4 |
| 7-8-9-12-24 | | |
| 7-8-9-12-25 | | |
| 7-8-9-13-16 | | |
| 7-8-9-13-17 | | |
| 7-8-9-13-18 | | |
| 7-8-9-13-19 | | |
| 7-8-9-13-20 | | |
| 7-8-9-13-21 | | |
| 7-8-9-13-22 | | |
| **Cluster for A atom diffusion** | **Figure** | **ECI (eV/cluster)** |
| 26-27-28-29-30 | | −0.1 |
| 26-27-28-29-31 | 4(c) | −0.1 |
| 26-27-28-29-32 | | −0.15 |
| 26-27-28-29-33 | | −0.2 |

## III. RESULTS AND DISCUSSION

### A. 2D square lattice

To clearly identify the effect of the local environment dependence of the KRA (EDKRA) barrier of the B-vacancy swap as expressed in the ABE LCE, we compare results with the case where all $E_{\mathrm{KRA}}$ for a B-vacancy swap is set to 0.6 eV (CTKRA). Of course, as described above, the $E_{\mathrm{KRA}}$ for an

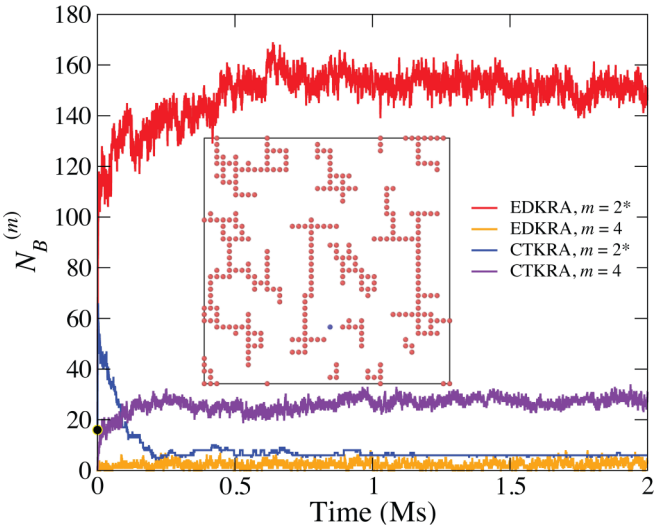


FIG. 5. Kinetic Monte Carlo simulation of short-range-order evolution in an A-B-vac alloy on a square lattice. Order parameters $N_B^{(2*)}$ and $N_B^{(4)}$ are shown as function of time for environmentally dependent kinetically resolved activation barriers (EDKRA) and configuration independent kinetically resolved activation barriers (CTKRA). The black circle on the vertical axis indicates the initial value of $N_B^{(2*)}$. The inset shows a characteristic configuration that is obtained with EDKRA after 2 Ms.

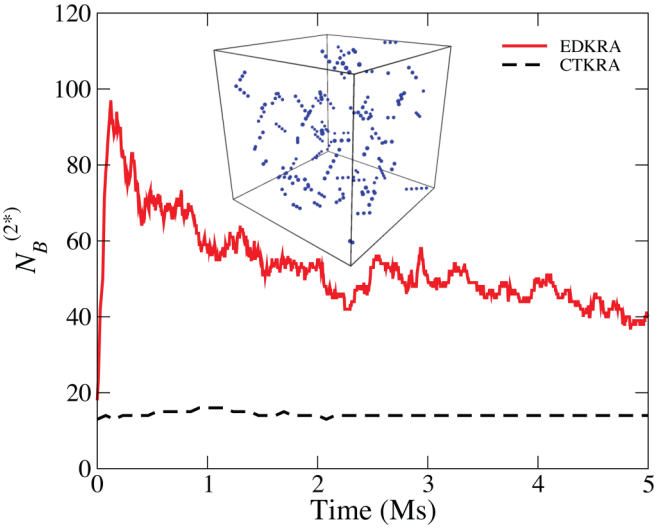


FIG. 6. Kinetic Monte Carlo simulation of short-range-order evolution in a phase separating $A_{0.95}B_{0.05}$ alloy with a single vacancy at 300 K. The simulation box consists of 20 × 20 × 20 conventional fcc cubes. The inset shows B atoms that are part of linear arrays of B atoms along the ⟨110⟩ direction after a simulation of 0.12 Ms in the EDKRA case.

A-vacancy swap is always 0.7 eV. To describe the evolution of the state of order, we define an order parameter $N_B^{(m)}$, which is the number of B atoms that has $m$ B neighbors. As we have designed our ABE LCE such that linear arrays of B atoms are preferred, we will define a special order parameter $N_B^{(2*)}$, which counts the number of B atoms that have precisely two B atoms in a straight line as neighbors.

Precipitation kinetics of an $A_{1279}B_{320}C$ alloy ($T = 300$ K) on a 2D 40 × 40 square lattice with periodic boundary conditions are shown in Fig. 5. Starting from a random configuration, the short-range order in the alloy is monitored through the $N_B^{(m)}$ order parameters as function of time. The kinetics in the EDKRA and the CTKRA cases are remarkably different. The CTKRA case exhibits the expected kinetics of B clusters forming from the random mixture: Isolated B atoms rather quickly connect with other B atoms to form clusters which coarsen over time. The number of twofold coordinated B atoms [$N_B^{(2*)}$] initially very rapidly increases, but then decreases as more B atoms join. The number of fourfold coordinated B atoms [$N_B^{(4)}$] follows a similar trend, but at a much slower pace. The EDKRA case, on the other hand, follows a completely different path. The inset shows a characteristic configuration after 2 Ms (Mega second), which features the linear B arrays with rather few side branches. As the value of $N_B^{(2*)} \approx 160$ shows, about half of all the B atoms (320) are in a linear configuration. After 2 Ms, $N_B^{(2*)}$ is about 30 times larger in the EDKRA than in the CTKRA case. The number of B atoms with four B neighbors in the inset is in the single digits and about one order of magnitude lower than in the CTKRA case. While there is no thermodynamic driving force that stabilizes the linear B arrays, these arrays nevertheless are robust for extremely long time periods, considering that 2 Ms corresponds to $2 \times 10^{18}$ jump attempts. We will show in the next section that the EDKRA kinetically drives the alloy toward transient states also persists in more realistic cases, such as on an fcc lattice in 3D.

### B. 3D FCC lattice

On the fcc lattice, we found here too a completely different behavior for EDKRA and CTKRA kinetics. Figure 6 shows the short-range-order evolution starting from the random configuration in a phase separating $A_{0.95}B_{0.05}$ alloy with a single vacancy at 300 K. The simulation is performed on a fixed fcc lattice containing $4 \times 20^3$ lattice sites with periodic boundary conditions. As shown in the inset of Fig. 6, there are many linear arrays of B atoms in ⟨110⟩ directions. This feature can also be seen from the peak of $N_B^{(2*)}$ after a time of about 0.12 Ms. In the random configuration $N_B^{(2*)} \approx 1600 \times 6 \times (0.05^2) \times (0.95^{10}) \approx 14$, a number that is seen for the CTKRA case is rather independent of time. As the barriers for B migration are not identical in the EDKRA and CTKRA case, it is worthwhile to consider if the two cases differ mostly in terms of timescale. Therefore, the time required for the CTKRA case to reach the same order parameter $N_B^{(m)}$ as the EDKRA at a particular time was examined. Two times were considered: EDKRA at $t = 42$ Ms and at $t = 150$ Ms as shown in Fig. 7. Data points below (above) the horizontal axis occur for B-atom coordinations that occur faster (slower) with EDKRA kinetics than with CTKRA kinetics. It is readily apparent that most configurations occur more quickly with EDKRA than with CTKRA kinetics, while the isolated B atoms, as indicated by $m = 0$, decay more rapidly. These findings occur both after 42 Ms and after 150 Ms have passed. However, B atoms with three B neighbors occur much quicker with CTKRA than with EDKRA kinetics. Therefore, EDKRA

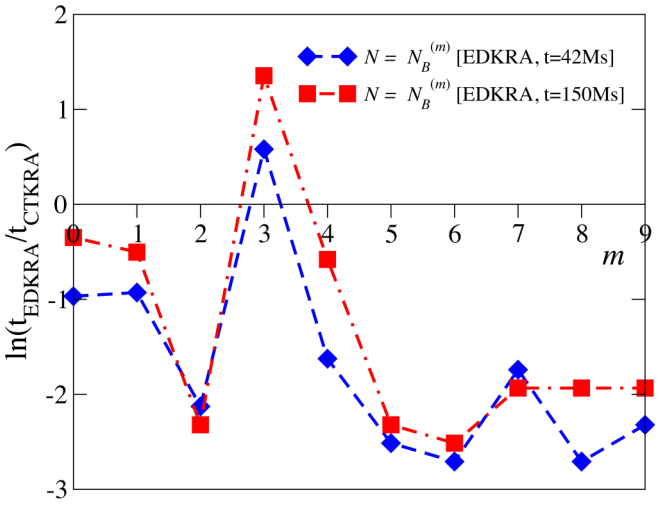


FIG. 7. The ratio of time required for EDKRA and CTKRA reaching the same values of $N_B^{(m)}$ as a function of $m$ after 42 Ms and after 150 Ms have passed with EDKRA kinetics.

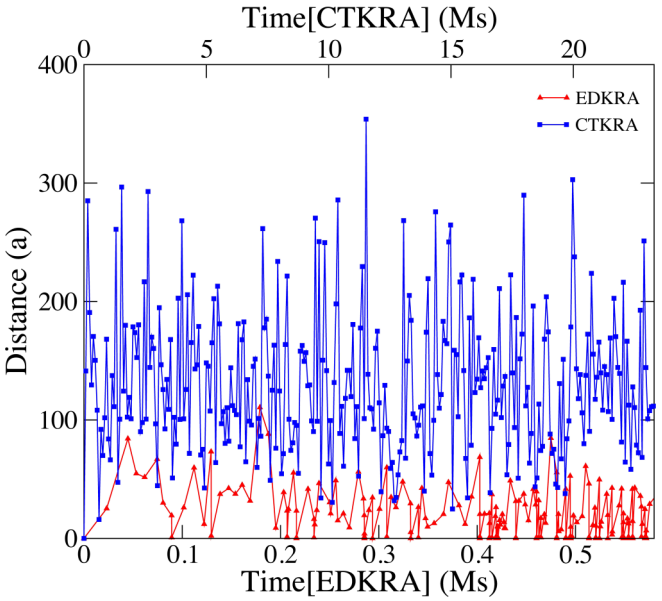


FIG. 8. Distance traveled, in units of the fcc lattice parameter, by a vacancy during successive intervals of 32 000 jumps for both EDKRA and CTKRA kinetics.

does not result in a general acceleration of kinetics, but in a different type of short-range-order evolution. The overall kinetics of the system described via EDKRA does not coincide with CTKRA, although initial states and thermodynamic equilibrium states are identical. This is similar to what was already observed for the 2D case.

Equation (3) shows that lowering the height of KRA barrier about 0.1 eV can speed up the vacancy-atom swapping by 50 times at room temperature. In several substitutional alloys, such as Al-Li [50,57] and Al-Cu [54] *ab initio* calculations have shown that KRA barriers are very sensitive to local configuration. In Al-Cu alloys, KRA barriers might vary by as much as a factor of 3 [54]. Especially at lower temperatures, this would result in kinetic pathways that strongly deviate from predictions obtained using configuration-independent KRA barriers. In multicomponent alloys such as the recently developed high entropy alloys (HEAs), the variety of the local atomic environment surrounding the multiple types of diffusing atoms becomes much more significant. The measured tracer diffusivities in HEAs indicate the diffusion activation barriers for various chemical orders can be quite different [58]. These results highlight the possibility of ordering phenomena purely driven by kinetics in actual alloys.

Another remarkable difference between EDKRA and CTKRA kinetics concerns vacancy mobility. In Fig. 8, the distance that a vacancy has moved during successive 32 000 atom swap intervals is shown for both EDKRA and CTKRA kinetics. It is apparent that the vacancy travels larger distances during CTKRA kinetics than during EDKRA kinetics. The reason for this behavior is that below average activation barriers in EDKRA, kinetics have the tendency to trap vacancies while no such trapping occurs in CTKRA. An example of such trapping can be seen in Fig. 3 where the vacancy, at least initially, will spend more time in positions $p_2$, $p_3$, and $p_4$ than in position $p_1$. The below-average barriers in EDKRA occur in the neighborhood of B atoms, and not in areas consisting purely of A atoms. As a consequence, the unproductive vacancy presence in pure A areas is much less in EDKRA than in CTKRA kinetics and the attachment of B atoms to B clusters proceeds at a greater rate with EDKRA kinetics. In previous work on Al-Li alloys [50], similarly, it was remarked that environmental dependence of diffusion activation barriers "induces strongly correlated migration mechanisms that deviate from random walk behavior."

## IV. CONCLUSIONS

Summarizing, we proposed an ordering mechanism in alloy systems where phase stability is thermodynamically characterized by phase separation. The essential requirement is that diffusion activation barriers in an alloy depend on the local environment. *Ab initio* density-functional calculations support this claim [50,54,57]. Furthermore, specific features in the local environment dependence of the diffusion activation barriers can give rise to peculiar short-range-ordered patterns that are not in any way related to a (meta)stable thermodynamic state. The kinetic activation barriers that lead to transient ordered states are fundamentally different from thermodynamic barriers because the latter scale with the size of the system while the former exist on the atomic scale only. The observed kinetically induced short-range-ordered configurations appear stable for extended time periods and thus can be considered transient phases. Our results also show that configurationally dependent activation barriers give rise to short-range-order evolution that cannot be reproduced by configuration independent activation barriers by, e.g., rescaling of time. The simulations have revealed a purely kinetic phenomenon of vacancy trapping that can accelerate the evolution of the short-range order in the alloy. It appears that to obtain

realistic descriptions of the kinetics of short-range ordering and precipitation in substitutional alloys, the environmental dependence of the diffusion activation barriers cannot be ignored.

**ACKNOWLEDGMENTS**

The authors gratefully acknowledge financial support from China Scholarship Council (CSC No. 2011637005). The authors thank Dr. Blazej Grabowski for discussions.

[1] T. D. Lee and C. N. Yang, Phys. Rev. **87**, 410 (1952).
[2] J. G. Amar, F. E. Sullivan, and R. D. Mountain, Phys. Rev. B **37**, 196 (1988).
[3] S. G. Brush, Rev. Mod. Phys. **39**, 883 (1967).
[4] C. V. Baal, Physica **64**, 571 (1973).
[5] R. Kikuchi, J. Sanchez, D. D. Fontaine, and H. Yamauchi, Acta Metall. **28**, 651 (1980).
[6] J. W. D. Connolly and A. R. Williams, Phys. Rev. B **27**, 5169 (1983).
[7] M. Sluiter and P. E. A. Turchi, Phys. Rev. B **40**, 11215 (1989).
[8] S.-H. Wei, L. G. Ferreira, and A. Zunger, Phys. Rev. B **41**, 8240 (1990).
[9] P. E. A. Turchi, M. Sluiter, F. J. Pinski, D. D. Johnson, D. M. Nicholson, G. M. Stocks, and J. B. Staunton, Phys. Rev. Lett. **67**, 1779 (1991).
[10] S. de Gironcoli, P. Giannozzi, and S. Baroni, Phys. Rev. Lett. **66**, 2116 (1991).
[11] M. Asta, D. de Fontaine, M. van Schilfgaarde, M. Sluiter, and M. Methfessel, Phys. Rev. B **46**, 5055 (1992).
[12] G. Ceder, Comput. Mater. Sci. **1**, 144 (1993).
[13] K. N. Ishihara, in *Non-equilibrium Processing of Materials*, edited by C. Suryanarayana, Pergamon Materials Series Vol. 2 (Elsevier Science, Oxford, 1999), pp. 5–20.
[14] E. Bévillon, J. P. Colombier, B. Dutta, and R. Stoian, J. Phys. Chem. Lett. **119**, 11438 (2015).
[15] S. Pogatscher, E. Kozeschnik, H. Antrekowitsch, M. Werinos, S. Gerstl, J. Löffler, and P. Uggowitzer, Scr. Mater. **89**, 53 (2014).
[16] S. Pogatscher, H. Antrekowitsch, M. Werinos, F. Moszner, S. S. A. Gerstl, M. F. Francis, W. A. Curtin, J. F. Löffler, and P. J. Uggowitzer, Phys. Rev. Lett. **112**, 225701 (2014).
[17] S. Wenner, K. Nishimura, K. Matsuda, T. Matsuzaki, D. Tomono, F. L. Pratt, C. D. Marioara, and R. Holmestad, Metall. Mater. Trans. A **45**, 5777 (2014).
[18] M. Werinos, H. Antrekowitsch, E. Kozeschnik, T. Ebner, F. Moszner, J. Löffler, P. Uggowitzer, and S. Pogatscher, Scr. Mater. **112**, 148 (2016).
[19] M. Werinos, H. Antrekowitsch, T. Ebner, R. Prillhofer, W. Curtin, P. Uggowitzer, and S. Pogatscher, Acta Mater. **118**, 296 (2016).
[20] A. J. Bray, Adv. Phys. **51**, 481 (2002).
[21] E. Vincent, C. Becquart, C. Pareige, P. Pareige, and C. Domain, J. Nucl. Mater. **373**, 387 (2008).
[22] D. M. B. Swoboda and A. van der Ven, J. Phase Equilib. Diffus. **31**, 250 (2010).
[23] N. Castin, G. Bonny, D. Terentyev, M. Lavrentiev, and D. Nguyen-Manh, J. Nucl. Mater. **417**, 1086 (2011), Proceedings of ICFRM-14.
[24] A. Van der Ven, G. Ceder, M. Asta, and P. D. Tepesch, Phys. Rev. B **64**, 184307 (2001).
[25] M. Leitner, D. Vogtenhuber, W. Pfeiler, and W. Püschl, Intermetallics **18**, 1091 (2010).
[26] D. R. Alfonso and D. N. Tafen, J. Phys. Chem. C. **118**, 22221 (2014).
[27] M. Francis and W. Curtin, Acta Mater. **106**, 117 (2016).
[28] J. S. Wróbel, D. Nguyen-Manh, K. J. Kurzydłowski, and S. L. Dudarev, J. Phys.: Condens. Matter **29**, 145403 (2017).
[29] H. M. Tawancy and M. O. Aboelfotoh, Phys. Status Solidi A **99**, 461 (1987).
[30] L.-Q. Chen, Y. Wang, and A. G. Khachaturyan, Philos. Mag. Lett. **64**, 241 (1991).
[31] C. Bansal, Z. Q. Gao, L. B. Hong, and B. Fultz, J. Appl. Phys. **76**, 5961 (1994).
[32] J. Ni and B. Gu, Phys. Rev. Lett. **79**, 3922 (1997).
[33] G. P. Srivastava, J. L. Martins, and A. Zunger, Phys. Rev. B **31**, 2561 (1985).
[34] C. Wolverton, V. Ozolins, and A. Zunger, J. Phys.: Condens. Matter **12**, 2749 (2000).
[35] H. Reichert, A. Schöps, I. B. Ramsteiner, V. N. Bugaev, O. Shchyglo, A. Udyansky, H. Dosch, M. Asta, R. Drautz, and V. Honkimäki, Phys. Rev. Lett. **95**, 235703 (2005).
[36] P. E. A. Turchi, L. T. Reinhard, and M. Sluiter, Int. J. Mod. Phys. B **07**, 286 (1993).
[37] L. Reinhard and P. E. A. Turchi, Phys. Rev. Lett. **72**, 120 (1994).
[38] F. Soisson and G. Martin, Phys. Rev. B **62**, 203 (2000).
[39] L.-Q. Chen and A. Khachaturyan, Acta Metall. Mater. **39**, 2533 (1991).
[40] B. S. Murty, D. H. Ping, and K. Hono, Appl. Phys. Lett. **77**, 1102 (2000).
[41] T. Ziller, G. Le Caër, O. Isnard, P. Cénédèse, and B. Fultz, Phys. Rev. B **65**, 024204 (2001).
[42] M. Styles, R. Marceau, T. Bastow, H. Brand, M. Gibson, and C. Hutchinson, Acta Mater. **98**, 64 (2015).
[43] D. Ma, M. Yao, K. Pradeep, C. C. Tasan, H. Springer, and D. Raabe, Acta Mater. **98**, 288 (2015).
[44] Y. Zheng, R. E. Williams, and H. L. Fraser, Scr. Mater. **113**, 202 (2016).
[45] R. Alert, P. Tierno, and J. Casademunt, Nat. Commun. **7**, 13067 (2016).
[46] L. Gao, X. Ding, T. Lookman, J. Sun, and E. K. H. Salje, Appl. Phys. Lett. **109**, 031912 (2016).
[47] D. Bochicchio, A. Videcoq, and R. Ferrando, Phys. Rev. E **87**, 022304 (2013).
[48] J. Perepezko, Prog. Mater. Sci. **49**, 263 (2004), a Festschrift in Honor of T. B. Massalski.
[49] A. D. Le Claire, Philos. Mag.: J. Theor. Exp. Appl. Phys. **21**, 819 (1970).
[50] A. Van der Ven and G. Ceder, Phys. Rev. Lett. **94**, 045901 (2005).
[51] F. Soisson and C.-C. Fu, Phys. Rev. B **76**, 214102 (2007).
[52] A. Van der Ven, H. Yu, G. Ceder, and K. Thornton, Prog. Mater. Sci. **55**, 61 (2010).

[53] X. Zhang and M. H. F. Sluiter, Phys. Rev. B **91**, 174107 (2015).
[54] X. Zhang and M. H. F. Sluiter, J. Phase Equilib. Diffus. **37**, 44 (2016).
[55] L. Onsager, Phys. Rev. **65**, 117 (1944).
[56] M. A. Novotny, Phys. Rev. Lett. **74**, 1 (1995).
[57] A. Van der Ven and G. Ceder, Phys. Rev. B **71**, 054102 (2005).
[58] M. Vaidya, K. G. Pradeep, B. S. Murty, G. Wilde, and S. V. Divinski, Acta Mater. **146**, 211 (2018).